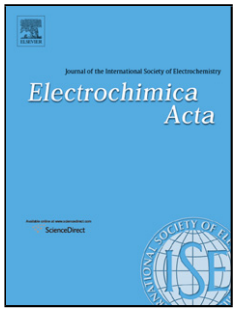

Title: Asymmetric supercapacitor devices based on dendritic conducting polymer and activated carbon

Authors: Darshna D. Potphode, Sarada P. Mishra, P. Sivaraman, Manoranjan Patri

PII: S0013-4686(17)30207-4
DOI: http://dx.doi.org/doi:10.1016/j.electacta.2017.01.168
Reference: EA 28835

To appear in: *Electrochimica Acta*

Received date: 25-10-2016
Revised date: 24-1-2017
Accepted date: 25-1-2017

Please cite this article as: Darshna D.Potphode, Sarada P.Mishra, P.Sivaraman, Manoranjan Patri, Asymmetric supercapacitor devices based on dendritic conducting polymer and activated carbon, Electrochimica Acta http://dx.doi.org/10.1016/j.electacta.2017.01.168

Asymmetric supercapacitor devices based on dendritic conducting polymer and activated carbon

Darshna D. Potphode, Sarada P. Mishra, P. Sivaraman, Manoranjan Patri*

Polymer Science and Technology Centre, Naval Materials Research Laboratory (DRDO), Shill-Badlapur Road, Anand Nagar P.O., Ambernath (E) 421506,Maharastra, India

Corresponding author. Tel.: +91 251 2623201; fax: +91 251 2623004.

E-mail address: mrpatri@gmail.com (M. Patri).

Graphical abstract

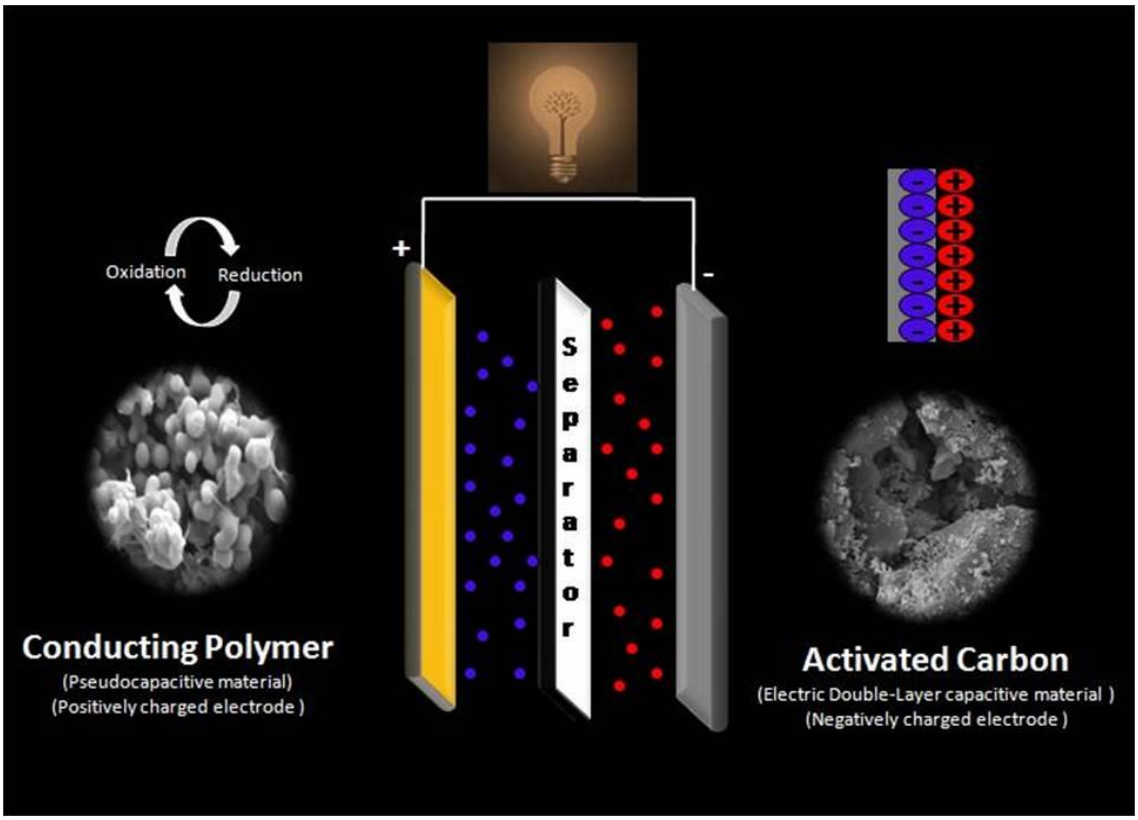

ABSTRACT

Dendritic conducting polymers(CPs) are a novel class of porous pseudocapacitive electrode materials assembled with the combination of highly reversible redox active triphenylamine(TPA) and thiophene, 3-methylthiophene, selenophene and thieno[3,2-b]thiophen moieties. Due to the unique combination of three dimensional conducting network, fast redox reversible reactions, porous morphology, high thermal and electrochemical stability have fetched these pseudocapacitive polymers to exhibit high specific capacitance and emerged as an ideal candidate for energy storage devices. The electrochemical performance of as-prepared polymers showed specific capacitance of 278, 257, 246 and 315 Fg^{-1} for poly tris[4-(2-thienyl)phenyl]amine (P1), poly tris(4-(3-methylthiophene-2-yl)phenyl)amine (P2), poly tris(4-(selenophen-2-yl)phenyl)amine (P3) and poly tris(4-thieno[3,2-b]thiophen-2-yl) phenyl)amine (P4) respectively with low internal resistance. An insertion of selenophene and thieno(3,2-b)thiophene linkers in TPA block showed enhanced electrochemical performance than the thiophene-TPA pair. Furthermore, asymmetric supercapacitors were assembled with the polymer as cathode and activated carbon as an anode and the detailed electrochemical characterizations has been investigated. This research may shed light on designing new redox active psuedocapacitors and other electrochemical devices.

Keywords: Triphenylamine, dendritic conducting polymers, energy storage, psuedocapacitors, asymmetric supercapacitors

1. INTRODUCTION

Supercapacitors are energy storage devices having capacity of bridging the gap between high energy density batteries and high power density conventional capacitors.[1] It can be used for harvesting energy and delivering high pulse power for short periods.[2,3] Depending upon the level and duration of the storage the electrode materials can be modified and used in many applications like hybrid vehicles, telecommunications, military weapons, spaceships etc.[4-8] For large scale practical application supercapacitors still suffer for low energy density as a major bottleneck. To overcome this, an asymmetric hybridization is considered as one of the most promising tact with psuedocapacitive material as the energy source and electric double layer capacitance material as the power source. This combination can offer outstanding energy density for whole system.[9]

The rapid growth in energy storage system demands advances in electrode materials for high specific capacitance and adequate stability. Carbon based electrode materials limits their use due to the non faradiac charge storage at the electrode-electrolyte interface which exhibits lower specific capacitance (~200 Fg^{-1}) than pseudocapacitive materials like metal oxides and CPs.[10-11] Pseudocapacitive materials are most promising materials since the charge storage in those can be induced by reversible redox reactions taking place at surface and bulk of the electrode.[12,13] Among pseudocapacitive materials,

metal oxides are potential candidates for higher specific capacitance (upto1200 Fg^{-1}) and high stability than the CPs but polymeric materials can compete them interms of low cost, easy route of synthesis, light weight etc as long as commercialization concern.[14-16] Further, the electrochemical properties of the conducting polymers can be tuned by controlling the chemical structure of the polymer by inexpensive ways than the metal oxides. The CPs, such as polyaniline, polypyrrole, polythiophene and their derivatives are widely studied for electrochemical energy storage in both aqueous and non aqueous systems.[13,17] Polyaniline, being most used polymer in electrochemical strorage, showed highest specific capacitance upto 815 Fg^{-1} with good environmental stability than the polypyrrole and polythiophenes.[16] Polythiophenes and its various derivatives have been well explored as electrode materials in supercapacitors with specific capacitance range of 180-250 Fg^{-1} in non-aqueous system.[18-19] Three dimentional structured TPA based materials are known for fast charge transfer and reversibly redox activity and have been utilized in various applications viz. organic field effect transistors, electrochromic devices, solar cells etc.[20,21] Moreover combination of TPA core with electron rich thiophene moiety to form a conducting polymer has been proved a potential electrode material for electrochemical storage.[22] Robert et al have reported electrochemically polymerized poly tris(4-(thiophene-2-yl) phenyl)amine based electrode material for energy storage. Nevertheless these kind of materials have not been fully explored for energy storage application. As polymeric structure and morphology plays an important role in energy storage,[23] incorporation of such

kind of materials in device fabrication has been receiving more attention due to their inherent redox properties and unusual high specific capacitance.[22]

In this work, the newer supercapacitor electrode materials have been developed by synthesizing of structurally homologous dendritic conducting polymers differing in the density of electron rich linkers (3-methyl thiophene, selenophene and thieno(3,2-b)thiophene) in direct conjugation with TPA core. As per aromaticity of the selenophene and thieno(3,2-b)thiophene concern, these polymer have been prepared following the idea that an aromatic system similar to the thiophene-TPA pair to exhibit superiority in contributing more quinoidal character and inter-ring π-electron delocalization in polymer backbone to enhance the electrochemical performance. The dendritic nature of the polymer plays an important role enhancing electrochemical storage to achieve highly porous morphology in the solid state by preventing close packing unlike linear chains. Moreover, our approach to creating the dendritic polymers through easy synthetic route by oxidative chemical polymerization has general applicability for large scale production at a very low cost and easy processible to use as electrode material in energy storage application.

2. Experimental

2.1 Materials

Thiophene, 3-methyl thiophene, selenophene, 2-isopropoxy-4,4,5,5-tetramethyl-1,3,2-dioxaborolane, ^{n}butyl lithium, tetrakis(triphenyl phosphine)palladium(0) ($Pd(PPh_3)_4$), unhydrous ferric chloride (anh.$FeCl_3$), potassium carbonate (K_2CO_3), acetonitrile (ACN) and tetraethylammonium

tetrafluoroborate ($TEABF_4$) were purchased from Sigma Aldrich and used as received. All solvents were dried by conventional methods prior to use. Activated carbon (AC) (surface area: 1990 $m^2\ g^{-1}$) used in the work was procured from PICA, France, grade:BP10. Conducting carbon (CC) powder (Vulcan XC-72) and carbon paper were procured from Cabot Corp., Japan and Toray, Japan respectively. Teflon (PTFE) suspension was supplied by Hindustan Flurocarbon Corp., India.

2.2 Instrumentation

The ^1H NMR spectra were recorded in a Brucker 400 FT-NMR spectrometer with chloroform-*d* as solvent. Chemical shifts were reported in ppm units with tetramethylsilane as an internal standard. Fourier transform infrared (FTIR) spectra of polymers were recorded in JASCO FT/IR–4200 over a scanning range from 500 to 4000 cm^{-1} using KBr pallets. Raman spectroscopy of the polymers was performed using Jobin Yovon spectrometer (HR 800 confocal micro Raman) on polymer powder samples with incident laser excitation wavelength of 514.5 nm. Thermogravimetric analysis (TGA; Hi Res TGA 2950, TA Instruments) of the polymers was carried out at a heating rate of 10 ℃ min^{-1} under nitrogen atmosphere. Field emission gun-scanning electron microscopic (FEG-SEM) analysis of polymers was conducted on a Carl Zeiss Supra-55VP field emission electron microscope. Electrochemical characterization was performed with an Ecochemie Autolab PGSTAT30 potentiostat.

2.3 Synthesis of monomers & polymers

Monomers were synthesized via Suzuki coupling reaction by following procedure reported elsewhere.[24] The general synthetic route for the monomers and polymers is shown in scheme 1.

Tris[4-(2-thienyl)phenyl]amine (monomer 1):

The tris (4-iodophenyl)amine (1.86g, 3mmol), 4,4,5,5-tetramethyl-2-(thiophen-2-yl)-1,3,2-dioxaborolane (2.2g, 10.5mmol) and $Pd(PPh_3)_4$ (0.34g, 0.3mmol) were dissolved in 200 mL of toluene. The solution was degased with N_2 for 30 min and then degasified solution of K_2CO_3 (6.73g, 44.9mmol) in 60 mL of H_2O was added. The mixture was refluxed for 24 h under inert atmosphere and cooled to rt. The compound was extracted in dichloromethane, washed with water, dried over $MgSO_4$ (anhd.) and evaporated. The purification was carried out using column chromatography (silica gel, petroleum ether as eluent) to obtain a yellow solid. **Yield**: 1 g (68.3%), Mp=138 ºC, ^{1}H NMR (400 MHz, $CDCl_3$) δ: 7.064 (d, *J*=2.4 Hz, 6H), 7.078 (d, *J*=2.4 Hz, 6H), 7.144 (d, *J*=5.6 Hz, 3H), 7.255 (d, *J*=7.6 Hz, 3H), 7.516 (d, *J*=5.6 Hz, 3H),

Tris(4-(3-methylthiophene-2-yl)phenyl)amine (monomer 2), Tris(4-(selenophen-2-yl)phenyl)amine (monomer 3) and Tris(4-thieno[3,2-b]thiophen-2-yl) phenyl) amine (monomer 4) were synthesized by following similar procedure.

Tris(4-(3-methylthiophene-2-yl)phenyl)amine (monomer 2): Yellow solid, Yield: 65%, Mp= 151 ºC, ^{1}H NMR (400 MHz, $CDCl_3$) δ: 2.36 (s, 9H), 6.94 (d, J=4 6H), 7.16 (d, J=6.8, 6H), 7.39 (d, J=6.4, 3H), 7.57 (d, J=6.8, 3H).

Tris(4-(selenophen-2-yl)phenyl)amine (monomer 3): Mustard-green solid, Yield: 43%, Mp=141 ºC, ^{1}H NMR (400 MHz, $CDCl_3$) δ: 7.16 (d, *J*=6.4 Hz, 6H), 7.3 (t, *J*=7.6 Hz, 3H), 7.45 (d, *J*=5.6 Hz, 3H), 7.56 (d, J=7.2, 6H), 7.91 (d, J=6.8, 3H).

Tris(4-thieno[3,2-b]thiophen-2-yl) phenyl) amine (monomer 4): Yellowish brown solid, Yield: 69%, Mp=179 ºC, ^{1}H NMR (400 MHz, CDCl3) δ:7.186 (d, *J*=6.8Hz, 6H), 7.252(d, *J*=4Hz, 6H), 7.349 (d, *J*=4Hz, 3H), 7.477 (d, *J*=4.8Hz, 3H), 7.558 (d, *J*=7.2 Hz, 3H).

Representative example of polymerization (P1)

To a $CHCl_3$ (6 mL) sloution of Tris[4-(2-thienyl)phenyl]amine (0.3g, 0.61mmol), suspension of anhydrous FeCl3 (0.495g, 3.05 mmol) in $CHCl_3$(4 mL) was added drop wise over 30 min. The reaction was continued at rt for addional 48h and then quenched with methanol. The residue was stirred in 5% methanolic solution of hydrazine hydrate (0.08 mmol) for 24h to dedope the polymer. Polymer was filtered, washed several times with methanol and soxhlet exctracted with methanol and acetone.

Poly tris[4-(2-thienyl)phenyl]amine (P1) Yield: 87%, IR (KBr, cm^{-1}) ν_{max} :3024, 1596, 1491, 1318, 1264, 1179, 1108, 966, 825, 730, 691

Polymers P2-P4 were synthesized and purified by similar procedure.

Poly tris(4-(3-methylthiophene-2-yl)phenyl)amine (P2) Yield: 96%, IR (KBr, cm^{-1}) ν_{max} :3070, 2921, 2853, 1597, 1482, 1314, 1268, 1180, 1109, 1005, 822, 721

Poly tris(4-(selenophen-2-yl)phenyl)amine (P3) Yield: 97%, IR (KBr, cm^{-1}) ν_{max} : 3024, 1589, 1488, 1316, 1277, 1180, 1106, 1004, 821, 727

Poly tris(4-thieno[3,2-b]thiophen-2-yl) phenyl) amine (P4) Yield: 85%, IR (KBr, cm^{-1}) ν_{max} :3078, 1596, 1486, 1320, 1283, 1176, 1014, 970, 810, 729, 637

2.4 Preparation of electrodes

Electrodes were fabricated by coating carbon paper with slurry of polymer or AC with CC in isopropyl alcohol and PTFE suspention(<5% of active material). The thickness of coating was maintained at 40±5 μm. The electrodes were then dried at 60 °C under vacuuo before using for electrochemical characterization. The electrodes of size 2 cm × 2 cm were prepared in which loading of active material was 1.25 mg cm^{-2}. The comppstion of electrode for both single electrode and two electrode characterisation is given in the table 1.

2.5 Device fabrication

Device was fabricated by using two electrodes of size 2 cm × 2 cm separated by capacitor grade paper. Positive electrode (cathode) was prepared with polymer material while negative electrode (anode) was with AC. Amount of AC in the negative electrode was kept constant (1.25 mg cm^{-2}) while polymer quantity was varied according to mass ratio of negative to positive electrode (γ_{max}).[25,26] Coating thickness were varied depending upon electrode mass

loading. The assembly was kept for drying in vacuum oven at 60°C for 8 h. It was sealed with plastic coated aluminium foil after addition of electrolyte. All the fabrication process was carried out in the glove box. Polymer/AC devices were named as PD1, PD2, PD3 and PD4 for P1/AC, P2/AC, P3/AC and P4/AC based compositions, respectively.

2.6 Electrochemical characterization

The electrochemical studies of asymmetric hybrid supercapacitors were studied by two electrode method in non-aqueous electrolyte (1M solution of $TEAFB_4$ in acetonitrile). In order to estimate the loading mass ratio of active materials in asymmetric hybrid supercapacitors, their individual specific capacitance was calculated by using three electrode configuration at initial stage where platinum mesh and Ag/AgCl were used as the counter electrode and reference electrode respectively. The electrochemical properties of the supercapacitor electrodes were studied by cyclic voltammetry (CV), galvanostatic charge–discharge (GCD) and electrochemical impedance spectroscopy (EIS). All the electrochemical measurements were carried out at room temperature using an Ecochemie Autolab PGSTAT30.

3. Results & Discussion

3.1 TGA

Thermogravimetric analysis (TGA) of the polymers indicates that all polymers are thermally stable upto 300°C with maximum 5% weight loss (Fig.1). At 300 °C, P1 showed only 0.7% weight loss. In P2, the incorporation of 3-methyl thiophene unit in place of thiophene shows typical degradation pattern with

enhanced thermal stability of the polymer. As the molecular structure determines the stability of polymer backbone, herein polymers are composed of highly rigid aromatic rings which imparts high thermal stability. P3 showed nearly similar weight loss pattern like P1 with quite high thermal stability while P4 is most stable among all polymers which could be ascribed to the highly rigid two fused thiophene rings therby contributing stability in polymer backbone. The carbonised residue (char yield) of these polymers were found to be 7.3%, 57%, 37.5% and 67% for P1, P2, P3 and P4 respectively at 800°C. The polymers P2-P4 showed higher thermal stability than the previously reported polymer P1, which could be attributed to the aromaticity of each individual linker.

3.2 Raman analysis

Fig. 2 shows the Raman spectra of the polymers. The highlighted region of Fig. 2 indicates the Raman active modes of polymers, indexing has been done according to the report by Hasoon et al. The major Raman active modes present in these polymers are Ag+B2g for □C-H(C-H in plane stretching of thiophene and selenophene), 2Ag+B2g for C-C ring stretching and Ag+B2g for C=C stretching.[27] The polymers P1 and P2 showed C-S bending peaks corresponding to the thiophene unit at 742 and 740 cm^{-1} respectively. In case of P3, C-Se bending is observed at 738 cm^{-1} while P4 shows two distinct peaks at 704 cm^{-1} and 733 cm^{-1} for C-S bending due to two fused thiophene rings. The peak at 1168 cm^{-1} in both P1 at P2 corresponds to C-H inplane stretching (Ag+B2g mode) of thiophene, P3 shows at 1176 cm^{-1} for C-H stretching of selenophene and P4 shows at 1136 and 1166 cm^{-1} respectively for thieno[3,2-

b]thiophen ring. The inter ring symmetric stretching of C_α-C_α is observed at 1185, 1182 and 1275 cm^{-1} in P1, P2 and P3 respectively and whereas for P4, two peaks observed at 1182 and 1201 cm^{-1}. The peaks at 1332, 1329, 1322 and 1347 cm^{-1} correspond to N-Ar-N stretching in P1, P2, P3 and P4 respectively. The symmetric ring stretching C_α-C_β (2Ag+B2g mode) of thiophene unit in P1 and P2 is observed at 1457 and 1465 cm^{-1} respectively, while P3 showed at 1457 cm^{-1} for selenophene and thieno[3,2-b]thiophen (P4) showed at 1481 cm^{-1}. The peaks at 1507, 1509, 1503 and 1520 cm^{-1} corresponds to C-C and C=C stretching of quinoid in P1, P2, P3 and P4 respectively. The C=C stretching (Ag+B2g mode) of benzonoid ring for P1, P2, P3 and P4 appears at 1607, 1602, 1603 and 1595 cm^{-1} respectively.[26-30] The functional group interpretation of the polymers from Raman spectra is corroborated with FTIR results which provided the evidence of polymerization.

3.3 SEM

SEM micrographs (Fig.3) showed the characteristic morphologies of polymers. The polymers P1, P3 and P4 exhibited porous structure assembled with small spherical particles of about 400 nm, on the other hand P2 showed highly porous polymer network. The molecular aggregation of the moieties causes the different morphologies of polymers which might be due to different molecular structures of TPA linkers. These well textured morphologies are expected to lead fast diffusion of ions inside the porous structure so that the

innermost active sites of electrode get doped to reduce the charge trapping during charge-discharge processes.

3.4 Electrochemical studies of Polymers

3.4.1. Cyclic Voltammetry (CV) studies

Fig. 4 shows the CV profile of polymers measured in 1 M $TEAFB_4$/ACN system in the potential window of 0 to 1.5 V at a scan rate of 25 mVs^{-1}. The electrochemical properties of the individual polymers were characterized by three electrode method (*vs* Ag/Agcl). The CV plots of each polymer electrode at different scan rates (i.e.10, 25, 50 and 100 mVs^{-1}) are given in Fig.1S. CV curves of polymers during p-doping exhibit a couple of anodic and cathodic peaks in quasi-reversible electron transfer pattern. P1-P4 showed anodic peak at 1.2V, 1.15V, 1.12V and 1.23 V while cathodic peak at -0.67V, -0.69V, -0.67V and -0.77V respectively. The potential difference between anodic and cathodic peak is 0.53V, 0.46V, 0.45V and 0.46V for P1, P2, P3 and P4 respectively. The lesser the potential difference faster will be the charge-discharge processes because of low charge transfer resistance at electrode-electrolyte interface and redox reaction tend to be diffusion controlled.[31] Difference in oxidation potential can be ascribed to difference in electronic density of thiophene, selenophene and thieno(3,2-b)thiophene linkers on polymer backbone. According to Cravino and co-workers, difference in π- electron distribution along the polymer backbone is responsible for the difference in lattice relaxation and vibrational behaviours of the CPs due to electron-phonon coupling,[32] which can be accountable for the

low energy band gap and the enhanced charge carrier capability of the polymers. The lowest oxidation potential of P3 is attributed to higher electron donating character of selenium atom than that of sulphur atom. An introduction of methyl group at thiophene linker also reduces oxidation potential of P2. Polymer P4 showed anodic/cathodic peaks at 1.23/-0.77V which is advantageous for broadening the electrochemical potential window in practical application. Hence polymers P2-P4 showed superior potential as electrode materials with fast redox reversibility than P1. The peak specific capacitance of 477, 520, 439 and 546 Fg^{-1} was achieved for P1, P2, P3 and P4 respectively. Whereas the actual specific capacitance obtained by integrating area under the curve is 271, 254, 243 and 310 Fg^{-1} for P1, P2, P3 and P4 respectively at scan rate of 25 mVs^{-1}. An alteration in thiophene linker by 3-methyl thiophene, selenophene and thieno(3,2-b)thiophene constitutes apparent change in specific capacitance of the polymers. The high specific capacitance and high redox reversibility during voltammetric scan are attributed to three dimensional structure of TPA core which helps to maintain good charge carrier pathway in polymer backbone as well as porous morphology for effective intercalation of electrolyte ions into the inner most part of the polymer chains. The prominent enhancement found in P4 can be attributed to thieno(3,2-b)thiophene linker for contributing more quinoidal character and therefore the π-electron inter-ring delocalization along the whole polymer.

3.4.2. Charge-discharge studies

The galvanostatic charge-discharge behavior of the as-prepared polymers was investigated at different current densities. The specific capacitance of the

polymers was calculated from the linear portion of discharge curve after IR drop using reported equation.[26] Triangular pseudocapacitive geometry and less IR drop in charge-discharge profile (Fig. 5) indicate their potential in energy storage. Polymer material in single electrode shows the specific capacitance of 278, 257, 246 and 315 Fg^{-1} for P1, P2, P3 and P4 respectively at 2.5 $mAcm^{-2}$ current density. These polymers showed high specific capacitance than the reported polythiophenes due to presence of easily oxidizable electron rich TPA moiety to form radical cation. The redox activity of the polymer backbone is responsible for the enhancement in faradic charge storage since these materials are known for fast electronic transport pathway.[33] The highest specific capacitance value for P4 is attributed to two fused thiophene ring attached to the TPA core which contributes more thiophene character to store the charge than the other polymers. The polymer P3 was expected to exhibit high specific capacitance than the P1 and P2. Elemental contribution of selenium with higher atomic size, easy polarization of selenophene unit and intermolecular Se-Se interaction than sulphur should enforce inter-chain charge transfer in polymer chain.[33] According to Asit et al. polyselenophenes are able to attain higher doping level than polythiophenes.[33] However it shows lesser specific capacitance than the other thiophene based polymers might be as a result of increase in intermolecular Se-Se distance in three dimensional dendritic structure.The specific capacitance of P3 obtained in this study is still higher than regular polythiophenes and polyselenophenes.[28]

3.5 Asymmetric device performance evaluation

3.5.1.CV of the asymmetric supercapacitor cell.

The supercapacitor cell capacitance is depends on voltage splitting across each electrodes which is mainly dependant on mass and specific capacitance of the active material used in each electrode. In symmetric supercapacitor the applied voltage can split equally between the two electrodes because of the same materials used in each electrodes with equal amount of active material. However in asymmetric supercapacitors the voltage split depends on the capacitance of the active material in each electrodes. Therefore to maintain the voltage equally, electrode mass was optimized according to report by Snook et al.[25] The coupling of electron rich aryl linkers with TPA core makes this combination more electron rich to give an efficient p-doping than n-doping. As these polymers are p-dopable, asymmetric supercapacitors have been assembled with polymers as a positive electrode materials and AC as a negative electrode. All the unit cells have been prepared by maintaining fixed amount of activated carbon (1.25 mg cm^{-2}) at negative electrode and amount of positive electrode active materaial was varied to maintain the mass ratio as per the reference [25]. Fig. 6 shows the CVs of AC electrode, polymer (P1) electrode and polymer/AC (PD1) unit cell at 25 mVs^{-1}. The asymmetric unit cell is scanned from 0 to 2.5 V, the potential sweep of negative (AC) electrode is varied from 0 to -1.5 V vs. Ag/Agcl and the positive (polymer) electrode is varied from 0 to 1.5 V vs. Ag/Agcl reference. The CV profile of AC electrode shows rectangular shape CV due to prominent electric double layer capacitance with coexitance of small

pseudocapacitance and the capacitance calculated from the CV profile was found to be ~100 F g^{-1}. As mentioned earlier, polymer CV is potential dependant due to prominent pseudocapacitance with minor electric double layer capacitance. As a result, the CV profile of the asymmetric unit cell is a collective contribution of these two capacitance. Below 1 V of the cell, the charge storage contribution by polymer electrode is comparatively less and hence the current response below 1 V is small. However once the oxidation potential of polymer is reached the current response of the cell increases and attains almost a plateau above 1V.

Fig. 7 shows the cyclic voltammogram of all hybrid AC/polymer devices at different scan rates viz. 10, 25, 50 and 100 mVs^{-1} in 1M TEATFB in acetonitrile. The specific capacitance of the cells was calculated using the equation 1.

$$Cell_{sc} = \frac{Q_1 + Q_2}{2mV} \quad \text{.....(1)}$$

where Q1 and Q2 are the sum of anodic and cathodic voltammetric charges during oxidation and reduction of the scans respectively, m is the mass of active material in both the electrodes of the cell and V is the potential difference. Q1 and Q2 value obtained by integrating the CV curve between 0.75 to 2.5 (V=1.75 V). The specific capacitance calculated for all polymer devices at various scan rates are given in the table 2. Even at high scan rate of 100 mVs^{-1}, the cells show ideal capacitive behaviour, which is desirable condition for fast charge-discharge of supercapacitor cells. The percentage change in capacitance values, when the

sweeping rate is change from 10 to 100 mVs^{-1} is the range of 13.0 to 16.9 %. This indicates that supercapacitor cells have high rate capability. The change in capacitance values between scan rates can be attributed to the following reasons. At lower scan rate, the high specific capacitance of unit cell is attributed to the lower concentration gradient at electrode/electrolyte interface which provides balanced doping and de-doping of active materials at respective electrodes. Hence the efficient redox reaction get active participation to cause enhancement in specific capacitance at lower scan rate. However at higher scan rate the concentration gradients at electrode/electrolyte interface increases and results an inadequate charge storage and causes lesser specific capacitance than lower scan rate.

3.5.2 Charge-discharge of unit cells

Since the unit cell performance was found to be appropriate in the voltage range of 1V to 2.5V in CV profile, charge-discharge profile was expected to show superior recital in the same range. Fig. 8 displays galvanostatic charge-discharge of the asymmetric cells carried out at current density of 0.5 Ag^{-1} in the potential range between 1V to 2.5V. The symmetry of the charge-discharge profile shows good capacitive behavior. The specific capacitance has been evaluated from the charge-discharge curves by following equation 1. The specific capacitance for asymmetric devices PD1, PD2, PD3 and PD4 was found to be 37.8, 37, 36.7 and 38.9 Fg^{-1}. All devices showed very negligible IR drop (~0.044 V) which attributes

to the fast redox reversibility of devices with remarkably low internal resistance. These results are corroborated with that obtained by cyclic voltammetric studies.

3.5.3 Impedance analysis of unit cells

To further investigate the charge transport and ion diffusion in the asymmetric supercapacitors based on dendritic conducting polymers we measured electrochemical impedance by EIS, from which their Nyquist plots were generated, as shown in Fig. 9. The x-intercept of the Nyquist plots represents the equivalent series resistance (ESR) for two-electrode supercapacitor and the charge transport resistance which is collective contribution of (i) discontinuity in the charge transfer process at the electrode-electrolyte interface (ii) intrinsic resistance of the active material (iii) contact resistance between the active material and current collector and (iv) resistance due to the faradic process.[35,36] Absence of semicircle in impedance plot (inset of Fig.9) is the evidence for the low internal resistance at the interface of electrode and current collector.[36] The slope of the Nyquist plots, known as the Warburg resistance, is a result of the frequency dependence of ion diffusion in the electrolyte to the electrode interface. As shown in Fig. 9, both the ESR and Warburg resistance of the all asymmetric supercapacitor are lower. The electrolytic resistance is almost same for all devices, indicating there is no much change in ionic conductivity since the morphology of the polymers is almost same. Three dimentional structures and the porous morphology of the polymers provides higher specifc electrochemical surface area which enhances the electrolyte penetration during redox reaction providing low Warburg impedance

since electrolyte diffusion get enhanced and contributes to reduce overall cell resistance. This also consistent with the results obtained from CV and Charge-discharge analysis which supports the diffusion control and fast redox reversible reactions at electrode-electrolyte interface.

5.4 Cycling studies

Further the supercapacitor devices were subjected to continuous charge-discharge cycles at constant current density of 0.5 Ag^{-1} to find out the electrochemical stability of the cells and the results are shown in Fig.10. As the electrochemical stability of AC is renowned up to ~5,00,000 cycles [37], the charge–discharge stability of asymmetric devices is significantly depends on polymer stability for at least up to number of cycles reported in this study. In particular, the cycling stability of PD2 and PD3 exhibits high initial degradation in specific capacitance while PD1 and PD2 are relatively stable. The values of specific capacitance loss during continuous charge-discharge for PD1, PD2, PD3 and PD4 are 24.6%, 33.2%, 32.9% and 21% respectively. Hence the electrochemical charge-discharge stability of device is greatly influenced by the stability of the polymer rather than AC. The highly porous morphology of the polymers which provides effective diffusion of electrolyte ions at electrode with less mechanical degradation. In practical, polymer stability can be explained on some major issues caused during charging-discharging processes, when polymers are subjected to continuous charge-discharge process they tends to acquire charge trapping because of compactness or re-aggregation caused due

to looser stacking micro-structure of polymer matrix which affects the degradation of polymer backbone. [13,34] These polymers showed higher electrochemical stability than conventional polythiophenes based electrode materials reported earlier.[38]

4.Conclusions

In summary, we synthesized a series of polymers containing TPA core and thiophene, 3-methyl thiophene, selenophene and thieno(3,2-b)thiophene linkers as a pseudocapacitive electrode materials for high-performance supercapacitor applications. TGA showed high thermal stability of the polymers. The microstuctured morphology of the polymers provided evidence to improved intercalation of electrolyte in electrode sites. The electrochemical studies of the polymers reveals that P4 (thieno(3,2-b)thiophene-TPA) showed highest specific capacitance and good electrochemical stability than the other polymers. Further, polymer/AC based asymmetric supercapacitors has been fabricated and electrochemically explored with CV, charge-discharge and impedance analysis. CV study showed specific capacitance of 38.5, 37.8, 37.6 and 39.0 Fg^{-1} for PD1-PD4 respectively which matched with theoretical and charge-discharge studies based calculations. FRA showed low internal resistance for all polymer devices with evidence for diffusion control and fast redox reversible reactions at electrode. These dentritic conducting polymer based electrode materials are proved to be promising entrant for energy storage applications.

References

[1] B.E. Conway, Electrochemical Supercapacitors, Scientific Fundamentals and Technological Applications, Kluwer Academic/Plenum Publishers, New York, USA, 1999.

[2] A. Burke, Ultracapacitors: why, how, and where is the technology, J. Power Sources 91 (2000) 37.

[3] L.L. Zhang, X. S. Zhao, Carbon-based materials as supercapacitor electrodes, Chem. Soc. Rev 38 (2009) 2520.

[4] K. Kotz, M. Carlen, Principles and Applications of Electrochemical Capacitors, Electrochim. Acta 45 (2000) 2483.

[5] G. Zhou, F. Li, H.-M. Cheng, Progress in flexible lthium batteries and future prospects Energy Environ. Sci. 7 (2014) 1307.

[6] D. H. Kim, J. Viventi, J. J. Amsden, J. Xiao, L. Vigeland, Y. S. Kim, J. A. Blanco, B. Panilaitis, E. S. Frechette, D. Contreras, D. L. Kaplan, F. G. Omenetto, Y. Huang, K. C. Hwang, M. R. Zakin, B. Litt, J. A. Rogers, Dissolvable films of silk fibroin for ultrathin conformal bio-integrated electronics. Nat. Mater. 9 (2010) 511.

[7] R. Li, B. Nie, P. Digiglio, T. Pan, Microflotronics: A Flexible, Transparent, Pressure-Sensitive Microfluidic Film, Adv. Funct. Mater. 24 (2014) 6195.

[8] P. Sivaraman, V.R. Hande, V.S. Mishra, C.S. Rao, A.B. Samui, All-solid supercapacitor based on polyaniline and sulfonated poly(ether ether ketone), J. Power Sources 124 (2003) 351.

[9] K. Naoi, W. Naoi, S. Aoyagi, H.-i. Miyamoto, T. Kamino, New Generation ″Nanohybrid Supercapacitor″, Acc. Chem. Res. 46 (2013) 1075.

[10] M. Inagaki, H. Konno, O. Tanaike, Carbon materials for electrochemical capacitors, J. Power Sources 195 (2010) 7880.

[11] D.D. Potphode, P. Sivaraman, S.P. Mishra, M. Patri, Polyaniline/partially exfoliated multi-walled carbon nanotubes based nanocomposites for supercapacitors, Electrochim. Acta 155 (2015) 402.

[12] C. Arbizzani, M. Mastragostino, F. Soavi, New Trends in Electrochemical Supercapacitors, J. Power Sources 100 (2001) 164.

[13] G. Wang, L. Zhang, A review of electrode materials for electrochemical supercapacitors, J. Chem.Soc.Rev. 41 (2012) 797.

[14] R. Ramya, R. Sivasubramanian, M.V. Sangaranarayanan, Conducting polymersbased electrochemical supercapacitors-Progress and prospects, Electrochim. Acta 101 (2013) 109.

[15] M. Mastragostino, C. Arbizzani, F.Soavi, Conducting polymers as electrode materials in supercapacitors, Solid State Ionics 148 (2002) 493.

[16] J. Heinze, B.A. Frontana-Uribe, S. Ludwigs, Electrochemistry of Conducting Polymerss Persistent Models and New Concepts, Chem. Rev. 110 (2010) 4724.

[17] G.A. Snook, P. Kao, A.S. Best, Conducting-polymer-based supercapacitor devices and electrodes, J. Power Sources 196 (2011) 1.

[18] M. Mastragostino, C. Arbizzani, F. Soavi, Polymer-based supercapacitors, J. Power Sources 97-98 (2001) 812.

[19] A. Laforgue, P. Simon, C. Sarrazin, J-F. Fauvarque, Polythiophene-based supercapacitors, J. Power Sources 80 (1999) 142.

[20] E. Ripaud, P. Leriche, N. Cocherel, T. Cauchy, P. Frere, J. Roncali, Tris thienylphenylamine –extended dithiafulvene hybrids as bifunctional electroactive species, J. Org. Biomol. Chem. 9 (2011) 1034.

[21] X. Cheng, J. Zhao, C. Cui, Y. Fu, X. Zhang, Star-shaped conjugated systems derived from thienyl-derivatized poly(triphenylamine)s as active materials for electrochromic devices, J. Electroanalytical Chemistry 677-680 (2012) 24.

[22] M.E. Roberts, D.R. Wheeler, B.B. McKenzie, B.C. Bunker, High specific capacitance conducting polymer supercapacitor electrodes based on poly (tris (thiophenylphenyl) amine), J. Mater. Chem 19 (2009) 6977.

[23] S. Nejati, T.E. Minford, Y.Y. Smolin, K.S. Lau, Enhanced charge storage of ultrathin polythiophene films within porous nanostructures, ACS NANO 8 (2014) 5413.

[24] W. Yang, J. Zhao, C. Cui, Y. Kong, P. Li, Characterization and Electrochemical Synthesize from Selenophene Substituted Poly(Triphenylamine) as Anodically Materials for Electrochromic Devices, Int. J. Electrochem. Sci. 7 (2012) 7960.

[25] G.A. Snook, G.J. Wilson, A.G. Pandolfo, Mathematical functions for optimisation of conducting polymer/activated carbon asymmetric supercapacitors, J. Power sources 186 (2009) 216.

[26] P. Sivaraman, A.R. Bhattacharya, S.P. Mishra, A.P. Thakur, Asymmetric supercapacitor containing poly (3-methyl thiophene)-multiwalled carbon

nanotubes nanocomposites and activated carbon, Electrochimica Acta. 94 (2013) 182.

[27] S. Hasoon, M. Galtier, J.L. Sauvajol, Vibrational modes of polythiophene and polyselenophene, Synth. Met. 28 (1989) C317.

[28]J. W. Park, S. J. Park, O. S. Kwon, C. Lee, J. Jang, In Situ Synthesis of Graphene/Polyselenophene Nanohybrid Materials as Highly Flexible Energy Storage Electrode, Chem. Mater. 26 (2014) 2354.

[29] C. Su, F. Yang, L. Ji, L. Xu, C. Zhang, Polytriphenylamine derivative with high free radical density as the novel organic cathode for lithium ion batteries, J. Mater. Chem. A 2 (2014) 20083.

[30] C. Kvarnstrom, A. Petr, P. Damlin, T. Lindfors, A. Ivaska, L. Dunsch, Raman and FTIR spectroscopic characterization of electrochemically synthesized Poly(triphenylamine), J Solid State Electrochem, 6 (2002) 505.

[31] O. A. Richard, M. Immaculate, S. Mantoa, A. A. Amir, T. Duarte, G. L. B. Priscilla, M.A.B. Christopher, K. Maher I. Emmanuel, Electrochemical Synthesis and Characterization of 1,2-Naphthaquinone-4-Sulfonic Acid Doped Polypyrrole, Electroanalysis, 19(2-3) (2007) 303.

[32] A. Cravino, H. Neugebauer, S. Luzzati, M. Catellani, A. Petr, L. Dunsch, N.S. Sariciftci, Positive and Negative Charge Carriers in Doped or Photoexcited Polydithienothiophenes: A Comparative Study Using Raman, Infrared, and Electron Spin Resonance Spectroscop, J. Phys. Chem. B, 106 (2002) 3583.

[33] A. Patra, M. Bendikov, Polyselenophenes, J. Mater.Chem. 20 (2010) 422.

[34] K. Naoi, M. Morita, Advanced polymers as active materials and electrolytes for electrochemical capacitors and hybrid capacitor systems, Electrochemic. Soc. Interface. 2008, 44.

[35] E. Barsoukov, J.R. Macdonald, Impedance Spectroscopy: Theory, Experiment, and Applications , John Wiley , New Jersey 2005 .

[36] P. Shobha, D. Muthu Gnana, T. Nathan, R. Mahesh, P. Sagayaraj, A comparative study on the structural and supercapacitive properties of TiO2 nanotubes fabricated by potentiostatic and galvanostatic anodization, Der Pharma Chemica 8(8) (2016) 64.

[37] S-E Chun, B. Evanko, X. Wang, D. Vonlanthen, X. Ji, G. D. Stucky, S. W. Boettcher, Design of aqueous redox-enhanced electrochemical capacitors with high specific energies and slow self-discharge, Nat. commun. 6:7818 (2015) 1.

[38] J. T. Kearns and M. E. Roberts, Synthesis of high-charge capacity triarylamine–thiophene redox electrodes using electrochemical copolymerization, J. Mater. Chem. 22 (2012) 25447.

Figure captions

1. TGA thermograms for polymers P1-P4 in N_2 at a scan rate of 10 °C min^{-1}.
2. Raman spectra of polymers P1-P4 measured at 514.5 nm.
3. SEM micrographs of polymers P1-P4.
4. CV curves normalized to specific capacitance for polymers P1-P4 (scan rate is 25 mVs^{-1}).
5. Galvanostatic charge-discharge curves for polymers P1-P4.
6. CV of polymer electrode, AC electrode and unit cell of Polymer-AC supercapacitor.
7. CV plots for polymer/AC devices at 10, 25, 50 and 100 mVs^{-1}.
8. Charge-discharge profile of polymer/AC devices at current density 0.5 Ag^{-1}
9. EIS of the polymer/AC based supercapacitor devices at different frequency. The inset shows EIS at high frequency end.
10. Charge-discharge cycling stability of polymer/AC devices

FIGURES

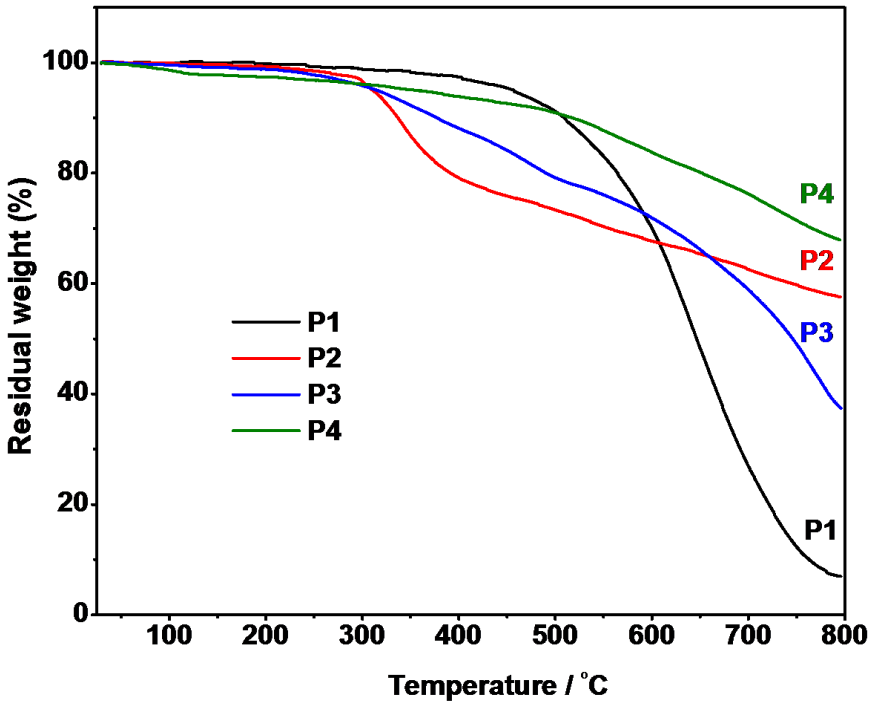

Figure 1

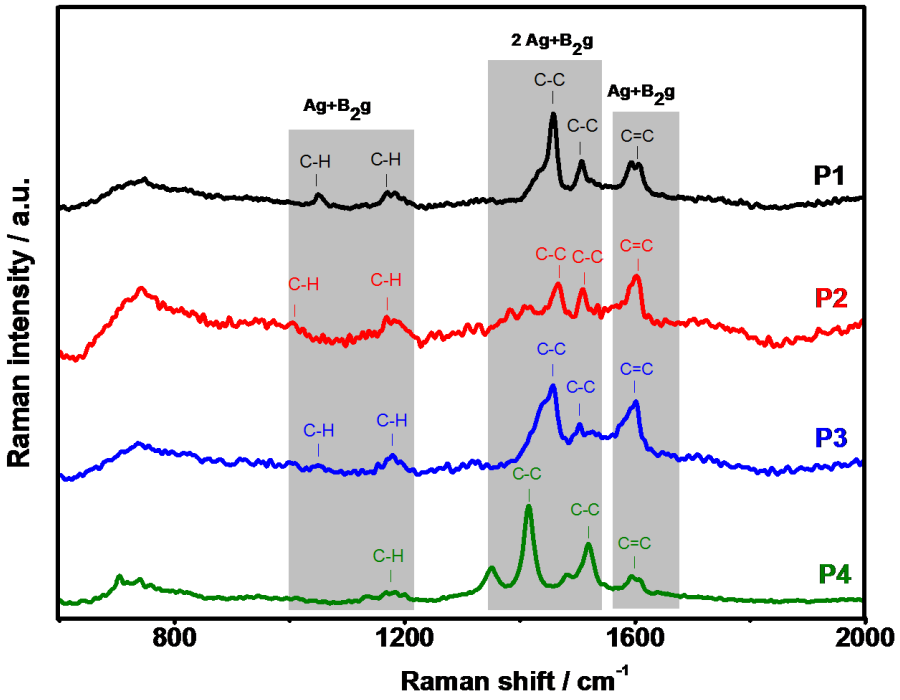

Figure 2

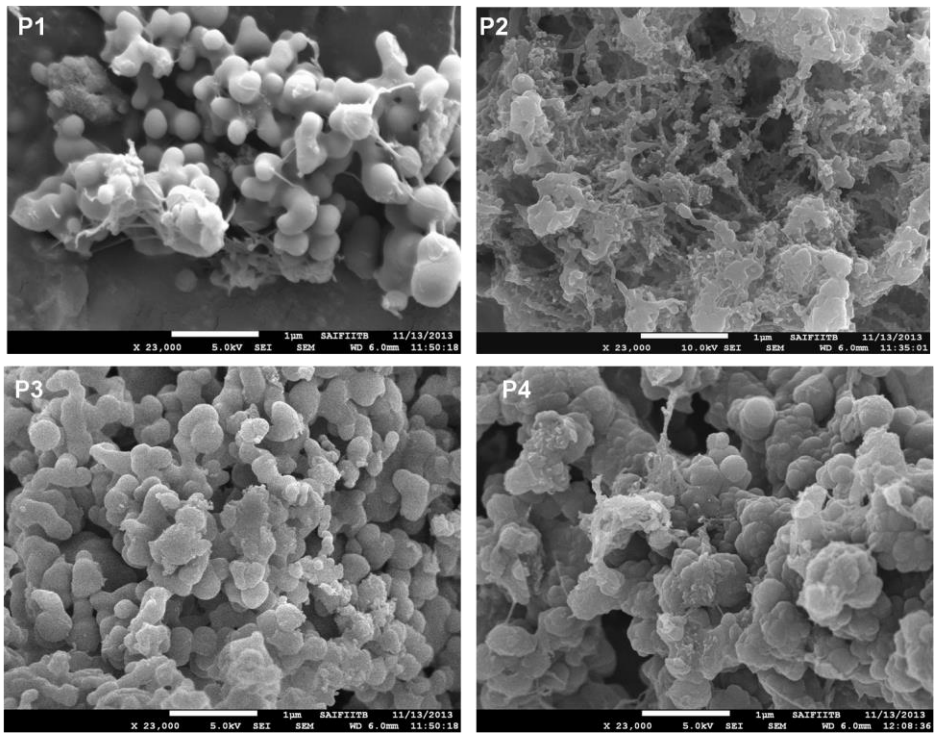

Figure 3

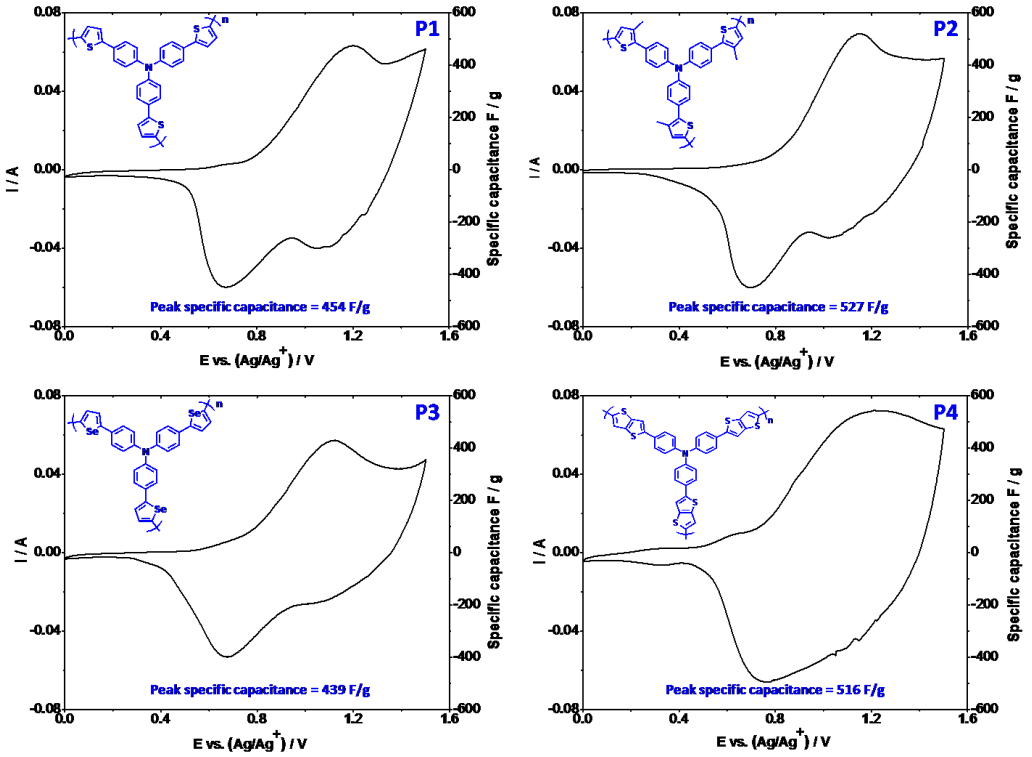

Figure 4

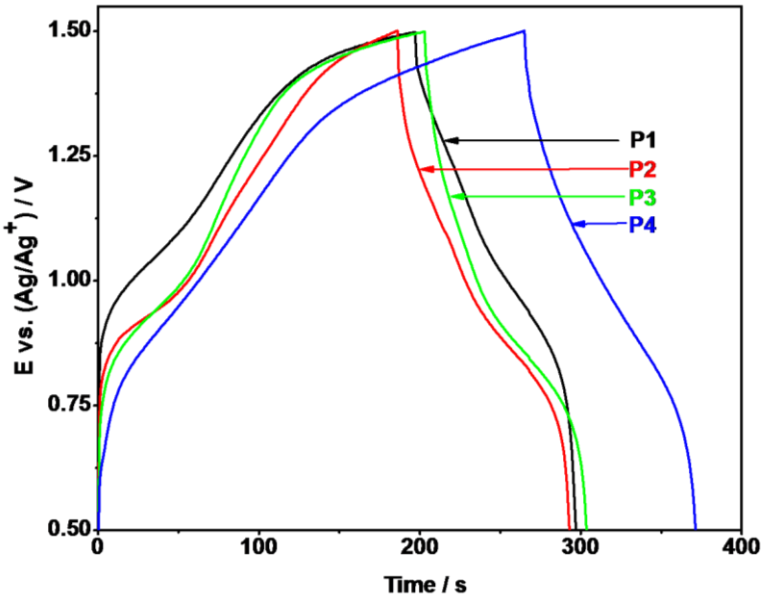

Figure 5

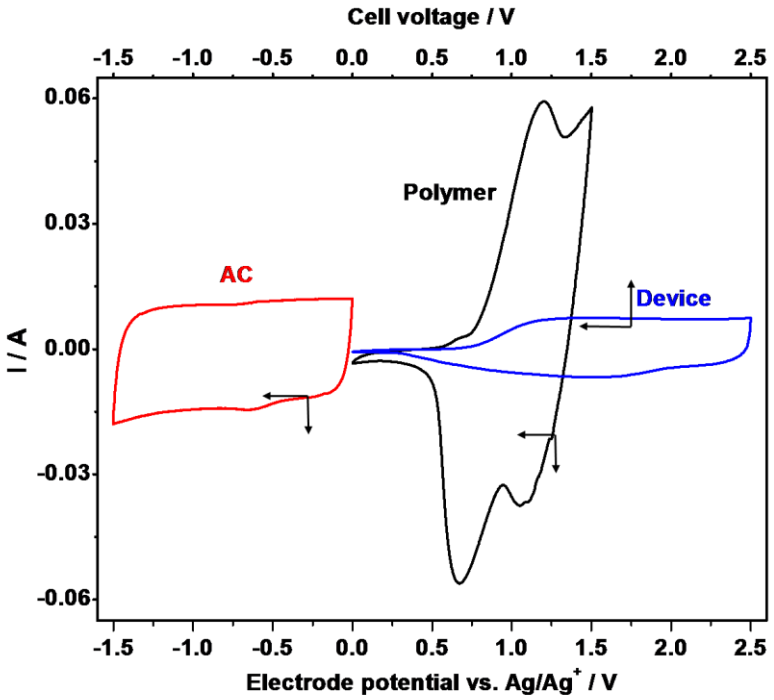

Figure 6

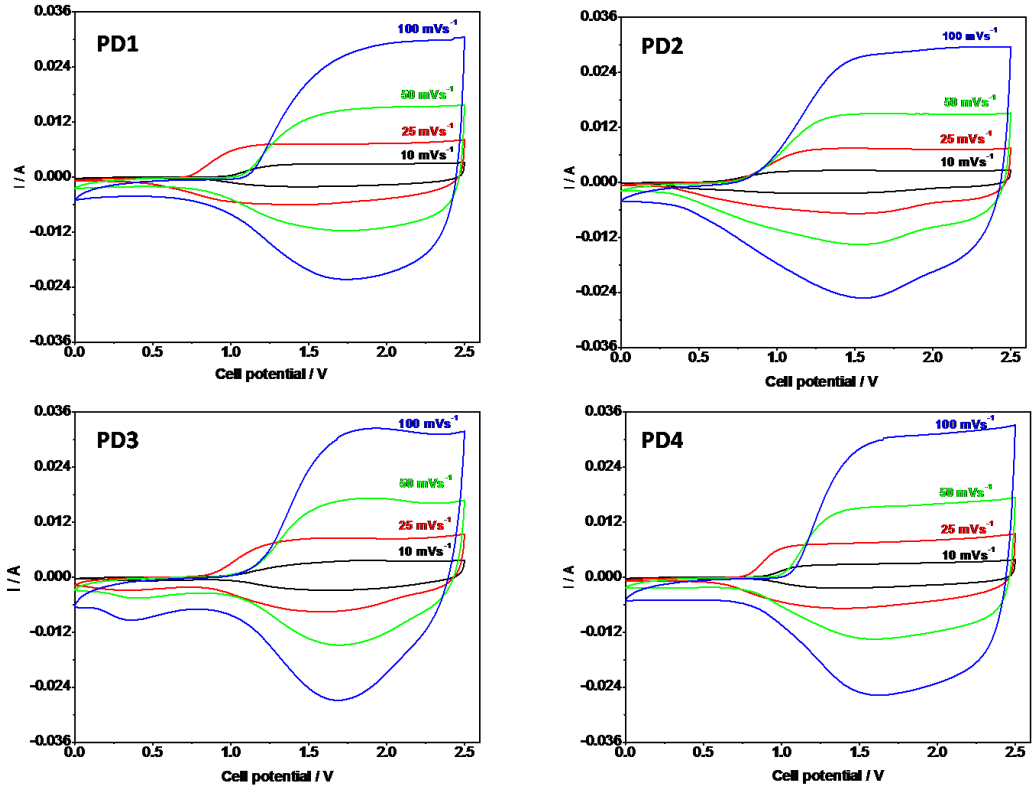

Figure 7

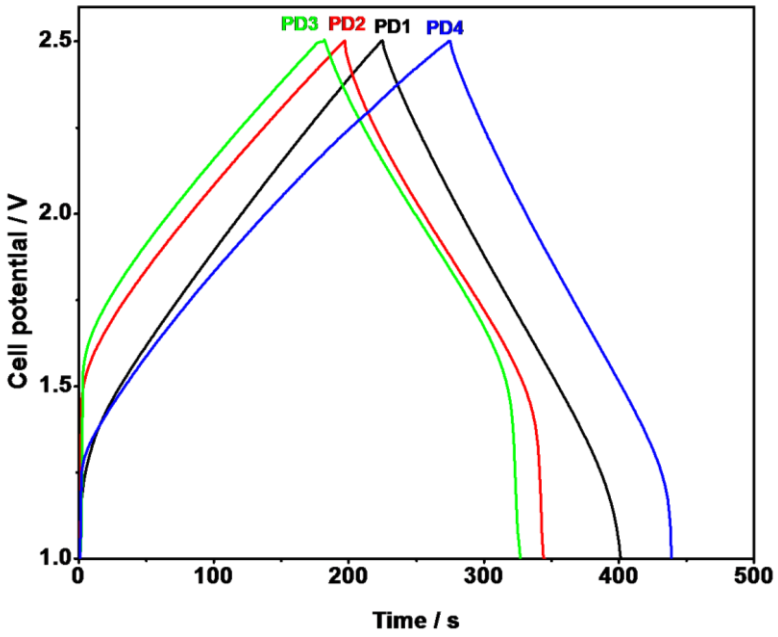

Figure 8

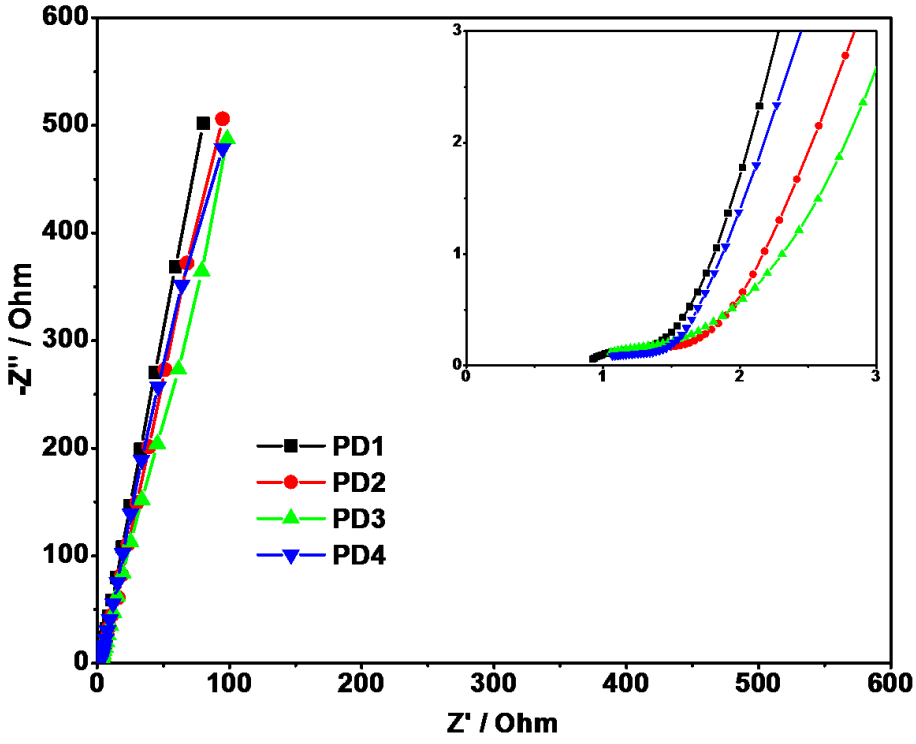

Figure 9

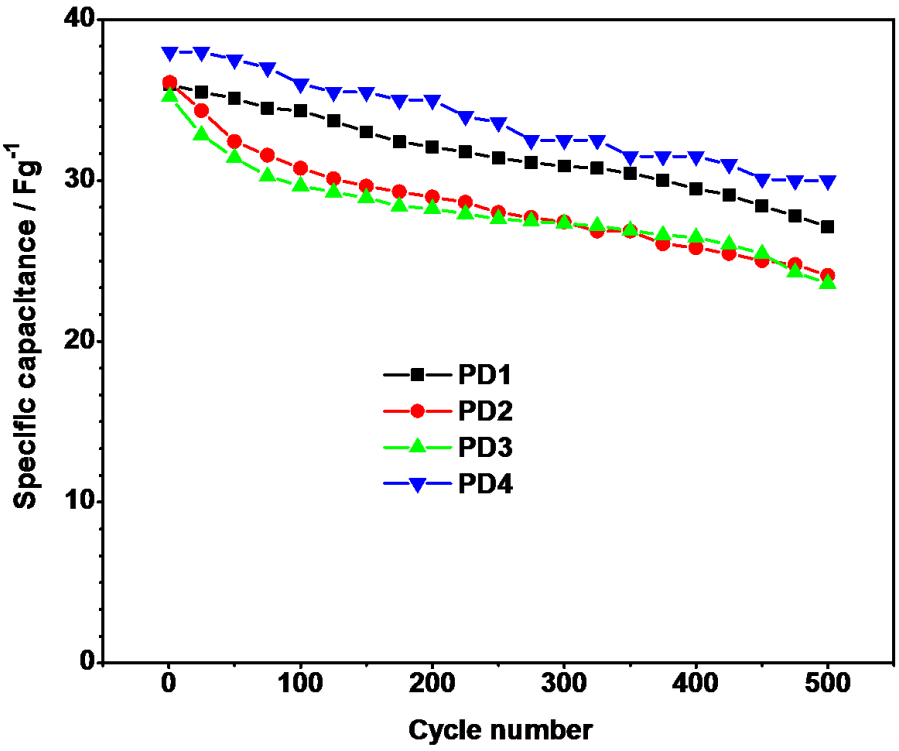

Figure 10

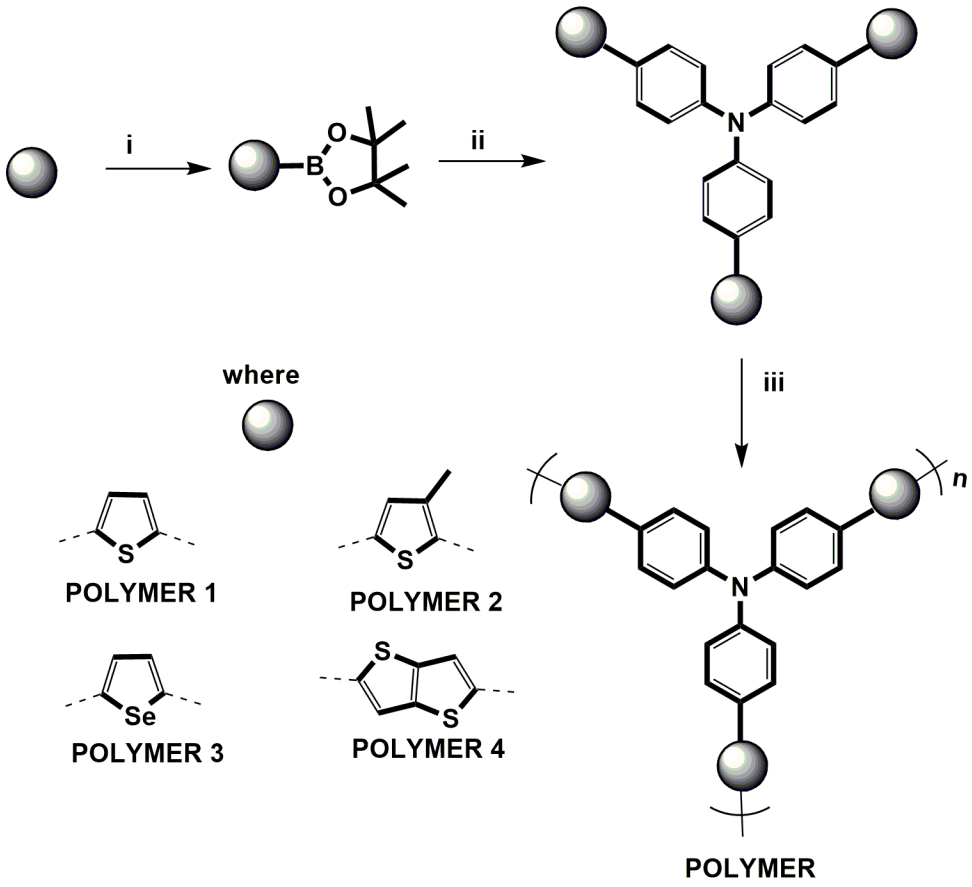

i) ^{n}BuLi, THF, -78 ^{0}C, dioxaborolane ii) Tri(4 iodophenyl)amine, K_2CO_3, $Pd(pph_3)_4$,Toluene, H_2O ,110 ^{o}C iii) anhy. $FeCl_3$, $CHCl_3$

Scheme 1. Schematic of monomer synthesis and polymerization.

Table 1: Electrode composition for supercapacitor

Electrode composition (weight ratio)	**P1**	**P2**	**P3**	**P4**	**AC**
Polymer	1	1	1	1	-
AC	-	-	-	-	1
CC	0.5	0.5	0.5	0.5	0.2
PTFE	0.05	0.05	0.05	0.05	0.05

Table 2: Specific capacitance of the devices at different scan rate.

Unit cell	10 mVs^{-1}	25 mVs^{-1}	50 mVs^{-1}	100 mVs^{-1}	Specific capacitance loss at 100 mVs^{-1}
PD1 (Fg^{-1})	38.5	35.2	33.9	32.0	16.9%
PD2 (Fg^{-1})	37.8	34.8	33.7	32.7	13.5%
PD3 (Fg^{-1})	37.6	36.7	34.8	32.6	13.3%
PD4 (Fg^{-1})	39.0	36.9	35.2	33.9	13.0%